Supplementary Information for

2D TeThCl with High Solar-to-Hydrogen Efficiency and Strain-Tunable Excitonic Properties

Calculation methods

(1) Young's modulus and Poisson's ratio

For 2D material, its in-plane Young's modulus (Y) and Poisson's ratio (υ) can be calculated using the formulas as follows:[1]

$$Y(\theta) = \frac{C_{11}C_{22} - C_{12}^2}{C_{11}\sin^4\theta + (\frac{C_{11}C_{22} - C_{12}^2}{C_{66}} - 2C_{12})\sin^2\theta\cos^2\theta + C_{22}\cos^4\theta}$$

(S1)

$$\upsilon(\theta) = \frac{C_{12}\sin^4\theta - (C_{11} + C_{22} - \frac{C_{11}C_{22} - C_{12}^2}{C_{66}})\sin^2\theta\cos^2\theta + C_{12}\cos^4\theta}{C_{11}\sin^4\theta + (\frac{C_{11}C_{22} - C_{12}^2}{C_{66}} - 2C_{12})\sin^2\theta\cos^2\theta + C_{22}\cos^4\theta}$$

(S2)

Where C_{ij} is the elastic constant, and θ is the angle with respect to a-axis.

(2) Carrier mobility

The carrier mobility (μ) can be calculated using the deformation potential theory (DPT) method, which can be described as:[2-4]

$$\mu = \frac{e\hbar^2 C^{2D}}{k_B T m^* m_d E_l^2}$$

(S3)

where C^{2D} is in-plane stiffness, m^* is the carrier effective mass, m_d is the density-of-states effective mass defined as $m_d = \sqrt{m_a^* m_b^*}$ (a and b represent the directions of the a-axis and b-axis), and E_l is the deformation potential constant defined by $E_l = \partial E_{edge}/\partial E$; E_{edge} is the energy near CBM (for electrons) and VBM (for holes), and E is the uniaxial strain along a-axis and b-axis. Here we set the total uniaxial strain is -2% ~ 2% and with the step size of 1%.

According to Lang et al. 's research[4], the acoustic phonon-limited mobility (APM, $\bar{\mu}$) of anisotropic 2D semiconductor can be corrected by its elastic constants (C_{ij}), which can be expressed as below:

$$\bar{\mu} = \frac{e\hbar^3}{k_B T (m_x^*)^{\frac{3}{2}}(m_y^*)^{\frac{1}{2}}} \left(\frac{A + B - \sqrt{A^2 - B^2}}{B\sqrt{A^2 - B^2}} \right) \times \left(\frac{I + J - \sqrt{I^2 - J^2}}{J\sqrt{I^2 - J^2}} \right)$$

(S4)

$$A = \bar{E}_l^2 + \frac{(\Delta E_l)^2}{2}, \quad B = \bar{E}_l \Delta E_l \qquad \text{(S5)}$$

$$\bar{E}_l = \frac{E_{lx} + E_{ly}}{2}, \quad \Delta E_l = \frac{E_{ly} - E_{lx}}{2} \qquad \text{(S6)}$$

$$\bar{C} = \frac{C_{11} + C_{22}}{2}, \quad \Delta C = \frac{C_{22} - C_{11}}{2} \qquad \text{(S7)}$$

$$I = \frac{1}{\sqrt{\bar{C}^2 - (\Delta C)^2}}, \quad J = \frac{\bar{C}}{\Delta C}\left(\frac{1}{\bar{C}} - \frac{1}{\sqrt{\bar{C}^2 - (\Delta C)^2}} \right) \qquad \text{(S8)}$$

(3) Gibbs free energy

We calculated the Gibbs free energy (ΔG) for the adsorption of intermediates (*H, *OH, *O, and *OOH) on the surface of the monolayer

during the photocatalytic water splitting process, governed by the following relationships:[5-7]

$$\Delta G = \Delta E + \Delta E_{ZPE} - T\Delta S + \Delta G_{pH} - eU \tag{S9}$$

Where ΔE represents the differential adsorption energy for each intermediate reaction, and ΔE_{ZPE} is the difference in zero-point energy (*ZPE*). *T* denotes the temperature of 298.15 K, while ΔS represents the entropy change obtained from vibrational frequency calculations. ΔG_{pH} accounts for the change in free energy influenced by the pH value. *U* is the electrode potential relative to the standard water reduction potential.

For HER, the expression for $T\Delta S$ is approximately −0.24 eV. Therefore, the Gibbs free energy *G of *H can be simplified as follows:

$$\Delta G_{*H} = \Delta E + 0.24 \tag{S10}$$

Fig. S1 Calculated cleavage energy (E_f, eV) of monolayer ThTeCl. The computation involves the total energies of the bulk unit cell (E_{bulk}, eV) and monolayer unit cell (E_{mono}, eV), and the in-plane area ($S_{in-plane}$, Å²). For comparison, the cleavage energies of monolayer graphene and MoS$_2$ are also provided.

| Materials	E_{bulk}	E_{mono}	$S_{in-plane}$	E_f
Graphene	-60.26	-19.98	5.26	0.33
MoS$_2$	-113.22	-56.46	8.81	0.27
RhTeCl	-322.19	-160.68	21.60	0.31
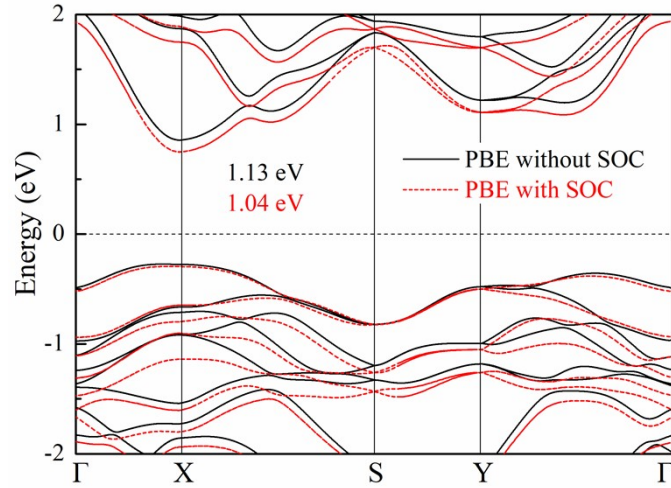
Fig. S1 Electronic band structures of the monolayer calculated using the PBE functional, with (red curve) and without (black curve) the inclusion of spin-orbit coupling (SOC).
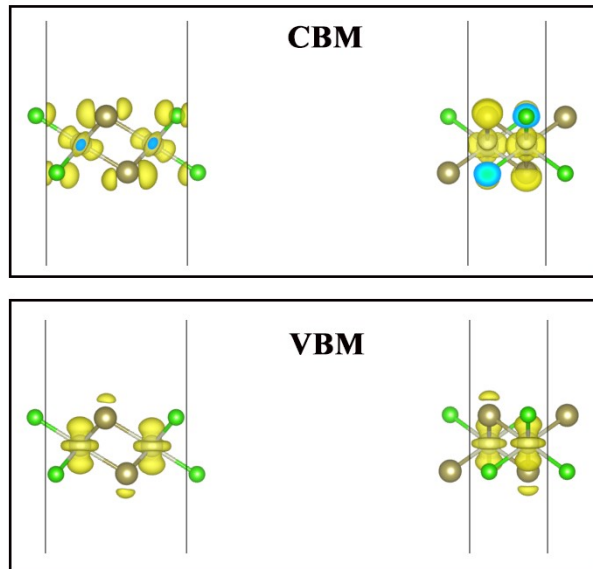

Fig. S2 Real-space distribution of the electron wave functions at the valence band maximum (VBM) and conduction band minimum (CBM) of monolayer ThTeCl. Two different side-view perspectives are provided.
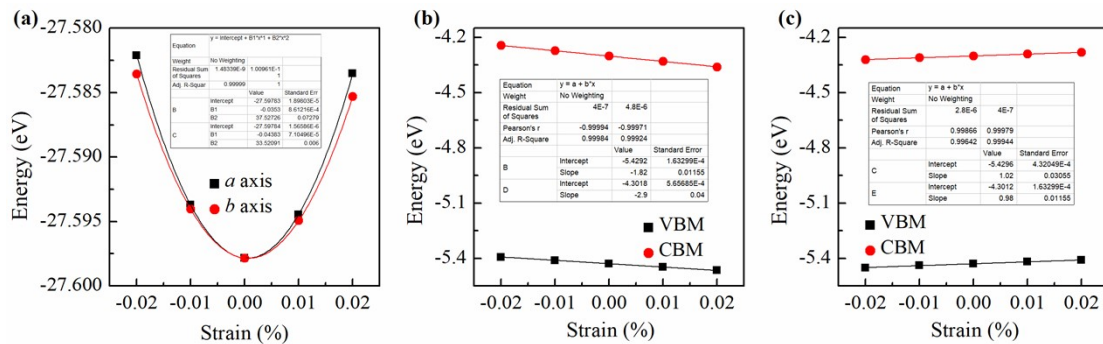

Fig. S3 Supporting data for the carrier mobility calculation within the deformation potential theory

framework. (a) The quadratic fitting of the total energy as a function of uniaxial strain, used to derive the planar stiffness. (b, c) Linear fittings of the VBM and CBM energies versus strain along the *a*- and *b*-axes, used to obtain the deformation potential constants for holes and electrons, respectively.
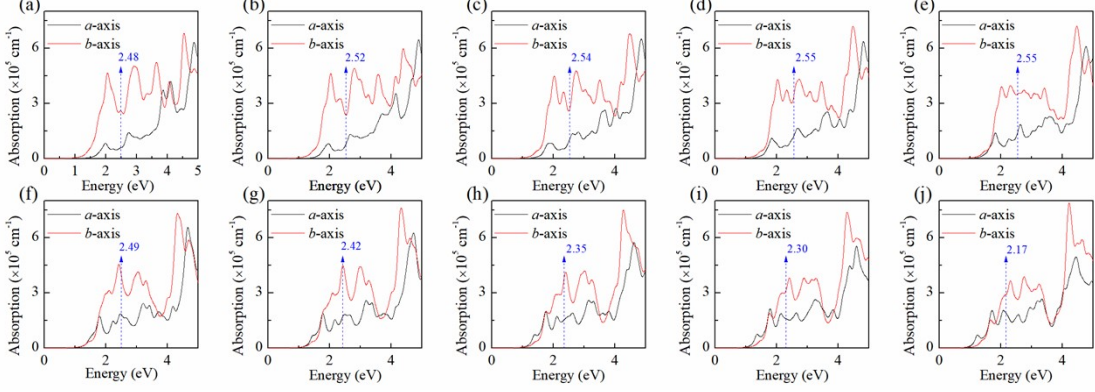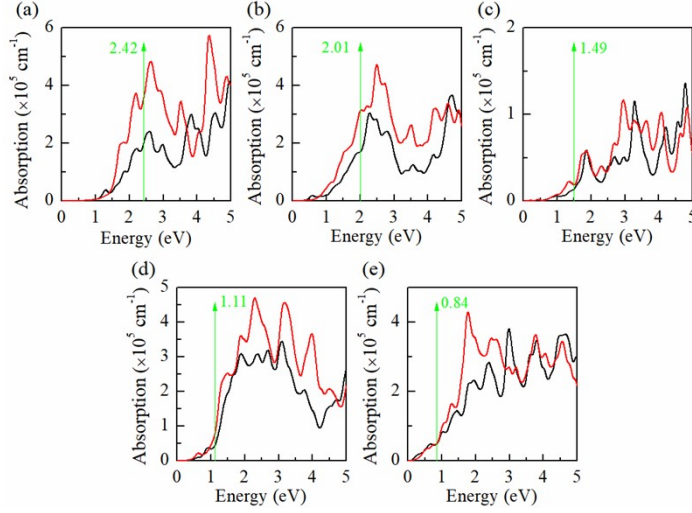

Fig. S4 Strain-tunable anisotropic optical absorption in monolayer RhTeCl. The absorption coefficients along the *a*-axis (black curves) and *b*-axis (red curves) are presented. The sequence from panel (a) to (j) illustrates the spectral evolution under uniaxial strain applied along the *a*-axis, ranging from -10% to +10% with a 2% step.
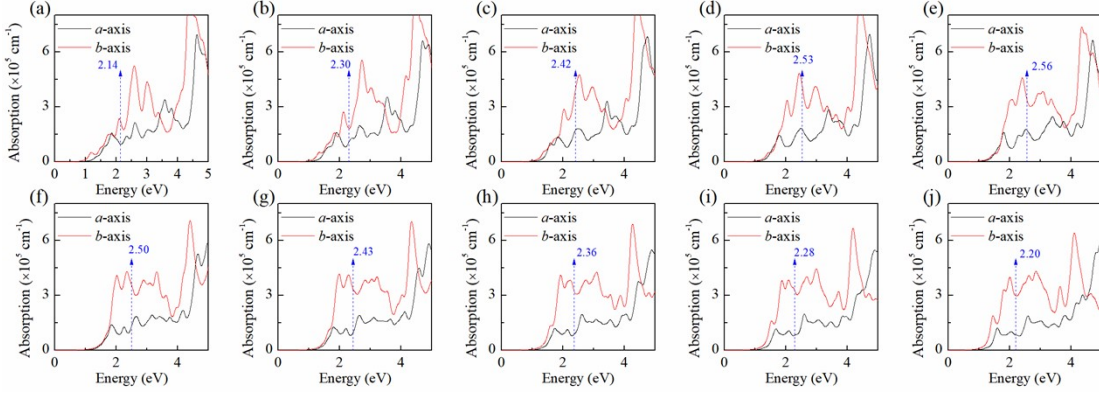
Fig. S5 Strain-tunable anisotropic optical absorption in monolayer RhTeCl. The absorption coefficients along the *a*-axis (black curves) and *b*-axis (red curves) are presented. The sequence from panel (a) to (j) illustrates the spectral evolution under uniaxial strain applied along the *b*-axis, ranging from -10% to +10% with a 2% step.
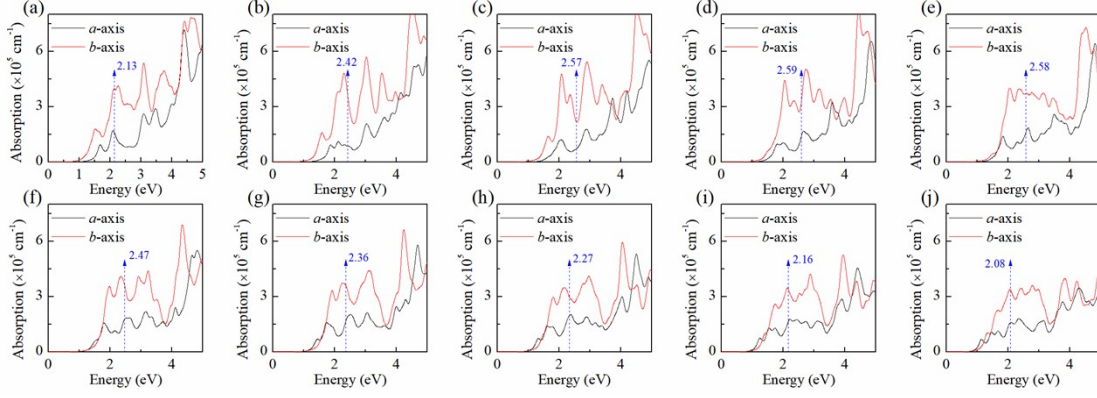
Fig. S6 Strain-tunable anisotropic optical absorption in monolayer RhTeCl. The absorption coefficients along the *a*-axis (black curves) and *b*-axis (red curves) are presented. The spectra from (a) to (j) correspond to the results under biaxial strain ranging from -10% to +10% with an increment of 2%.

Fig. S7 Modulation of the anisotropic optical absorption in monolayer RhTeCl by an external electric field. The absorption coefficients along the *a*-axis (black curves) and *b*-axis (red curves) are presented. The sequence from panel (a) to (e) corresponds to the calculated spectra under electric fields of 0.1, 0.2, 0.3, 0.4, and 0.5 V/Å, respectively.

Table S2 The total energy E_t, the position of VBM (E_V) and CBM (E_C) with respect to vacuum level at uniaxial strains of -4% ~ 4%, where the step size is 1%.

Direction	Strain	E_t (eV)	E_V (eV)	E_C (eV)
a-axis	-4%	-27.582	-5.393	-4.245
	-2%	-27.594	-5.411	-4.272
	0%	-27.598	-5.429	-4.301
	2%	-27.594	-5.447	-4.330
	4%	-27.584	-5.466	-4.361
b-axis	-4%	-27.584	-5.451	-4.321
	-2%	-27.594	-5.439	-4.311
	0%	-27.598	-5.429	-4.301
	2%	-27.595	-5.419	-4.291

4%	-27.585	-5.410	-4.282

Table S3 The calculation details of the Gibbs free energy change of the intermediate product in monolayer during the OER. Here, E_{DFT} represents the total energy of the intermediate product adsorbed at the most probable position on the superlattice surface, G_{tot} represents the total Gibbs free energy, and the T is set to 298.15 K.

Materials	E_{DFT}	ΔE_{zpe}	$T\Delta S$	Molecular	G_{tot}	ΔG ($U = 0.0$ V)	ΔG ($U = 1.23$ V)
G*	-165.657	0.000	0.000	H_2O	-194.125	0.000	0.000
G*OH	-174.829	0.318	0.163	$H_2O + (H^+ + e^-)$	-192.311	1.815	0.585
G*O	-170.711	0.062	0.080	$H_2O + 2(H^+ + e^-)$	-191.770	2.355	-0.105
G*OOH	-179.008	0.406	0.193	$3(H^+ + e^-)$	-189.005	5.120	1.430
G*	-165.657	0.000	0.000	$O_2 + 4(H^+ + e^-)$	-189.205	4.920	0.000

References

[1] W Y Fang, X L Xiao, H R Wei, Y Chen, M K Li, Y B He. The elastic, electron, phonon, and vibrational properties of monolayer XO_2 (X = Cr, Mo, W) from first principles calculations, Materials Today Communications 30 (2022), http://dx.doi.org/10.1016/j.mtcomm.2022.103183.

[2] W Y Fang, K Kuang, X L Xiao, H R Wei, Y Chen, M K Li, Y B He. Ab initio study of two-dimensional $MgAl_2Se_4$ and $MgIn_2Se_4$ with high stability, high electron mobility, and high thermoelectric figure of merit, Journal of Alloys and Compounds 931 (2023), http://dx.doi.org/10.1016/j.jallcom.2022.167586.

[3] M J Varjovi, M E Kilic, E Durgun. Ternary pentagonal BNSi monolayer: Two-dimensional structure with potentially high carrier mobility and strong excitonic effects for photocatalytic applications, Physical Review Materials 6 (3) (2022), http://dx.doi.org/10.1103/PhysRevMaterials.6.034004.

[4] H F Lang, S Q Zhang, Z R Liu. Mobility anisotropy of two-dimensional semiconductors, Physical Review B 94 (23) (2016), 235306, http://dx.doi.org/10.1103/PhysRevB.94.235306.

[5] G L Qian, Q Xie, Q Liang, X Y Luo, Y X Wang. Electronic properties and photocatalytic water splitting with high solar-to-hydrogen efficiency in a hBNC/Janus WSSe heterojunction: First-principles calculations, Physical Review B 107 (15) (2023), 155306, http://dx.doi.org/10.1103/PhysRevB.107.155306.

[6] H Li, C Xu, H Hu, F Dai, W Fang. Computational study of the photocatalytic water splitting performance of two-dimensional PdSeO3, Inorganic Chemistry Communications 178 (2025), 114510 http://dx.doi.org/10.1016/j.inoche.2025.114510.

[7] DanChen, Pei-genFang, J-l Bai, W-y Fang, Sheng-anChen, KaiJin. Computational investigation of high stability and solar-to-hydrogen efficiency in two-dimensional SiP, GeP, and SnP for enhanced

photocatalytic water splitting, Journal of Materials Chemistry A 13 (2025), 17622-17628, http://dx.doi.org/10.1039/D5TA01657F.